Supporting Information for

Polymorphism modulates photoluminescence and magnetic dynamics of mononuclear dysprosium-anthracene complexes

Xiu-Fang Ma, [†] Ying Guo, [‡] Xin-Da Huang, [†] Ge-Hua Wen, [†] Song-Song Bao, [†] Yi-Quan Zhang*,[‡] and Li-Min Zheng*,[†]

[†]State Key Laboratory of Coordination Chemistry, School of Chemistry and Chemical Engineering, Collaborative Innovation Center of Advanced Microstructures, Nanjing University, Nanjing 210023, P. R. China.

[‡]Jiangsu Key Laboratory for NSLSCS, School of Physical Science and Technology, Nanjing Normal University, Nanjing 210023, P. R. China.

*correspondence to: lmzheng@nju.edu.cn, zhangyiquan@njnu.edu.cn

Contents

I. Materials, methods and syntheses

Materials and Physical Measurements

The ligand 9-diethyl-phosphonomethylanthracene (depma) was synthesized according to the literature.[1] All the other reagents and solvents obtained from commercial channels were of analytical grade. The C and H microanalyses were performed on PE 240C analyzer. The infrared spectra were measured in the range 400-4000 cm^{-1} using KBr pellets on Bruker Tensor 27 spectrometer. The thermogravimetric analysis was conducted using a Mettler-Toledo TGA/DSC STARe thermal analyzer under N_2 atmosphere at a heating rate of 5 °C min^{-1} from 30 to 600 °C. Powder X-ray diffraction patterns (PXRD) were performed on a Bruker D8 advance diffractometer using Cu-Kα radiation in a range of 5-50° at room temperature. The dc and ac magnetic susceptibility data were obtained using polycrystalline samples by a Quantum Design SQUID VSM magnetometer. The UV/Vis spectra were measured on a PerkinElmer Lambda 950 UV/VIS/NIR spectrometer using powder samples. The steady fluorescence spectra were attained with Spectrofluorimeter PE LS55. Time resolved fluorescence and quantum yield measurements were performed on an Edinburgh FLS 980 at room temperature.

Preparation of complexes α-DyCl, β-DyCl and β-DyBr

Synthesis of α-DyCl and β-DyCl. A CH_3CN (6 mL) solution of $DyCl_3·6H_2O$ (0.05 mmol, 18.8 mg), depma (0.15 mmol, 49.3 mg) was kept in a pressure glass reaction tube at 75 °C for 24h. After cooling to room temperature, filtered and left in glove box at room temperature for three days to afford a mixture of the polymorphs **α-DyCl** and **β-DyCl**. Furthermore, visual inspection of a large number of identically prepared reaction solutions showed that **α-DyCl** and **β-DyCl** were formed in different proportions each time. Polymorphic crystals can be hand-separated under a microscope due to significant differences in emission color under UV light (lime green for **α-DyCl** and yellowish green for **β-DyCl**, respectively).

Data for **α-DyCl**. Yield: 26.7 mg (42.6%). Elemental analysis calcd (%) for $C_{57}H_{63}Cl_3DyO_9P_3$: C, 54.60; H, 5.06. Found (%): C, 54.57; H, 5.07. IR (KBr, cm^{-1}): 3050(w), 2985(w), 2946(w), 2905(w), 1623(m), 1529(w), 1448(w), 1410(w), 1393(w), 1347(w), 1383(w), 1252(w), 1202(m),

1197(w), 1168(vs), 1145(vs), 1099(w), 1053(vs), 1033 (vs), 984(w), 958(w), 932(w), 914(w), 888(w), 825(w), 783(m), 737(w), 695(w), 629(w), 603(w), 571(w), 542(w), 508(w).

Data for **β-DyCl**. Yield: 37.4 mg (59.7%). Elemental analysis calcd (%) for $C_{57}H_{63}Cl_3DyO_9P_3$: C, 54.60; H, 5.06. Found (%): C, 54.59; H, 5.16. IR (KBr, cm^{-1}): 3050(w), 2985(w), 2946(w), 2904(w), 1623(m), 1529(w), 1448(w), 1410(w), 1393(w), 1370(w), 1347(w), 1283(w), 1253(w), 1175(vs), 1051(vs), 1028(vs), 974(w), 929(w), 891(w), 819(w), 784(w), 735(m), 692(w), 641(w), 603(w), 571(w), 539(w), 502(w).

Synthesis of β-DyBr. A CH_3CN (6 mL) solution of $DyBr_3·H_2O$ (0.05 mmol, 21.1 mg), depma (0.15 mmol, 49.3 mg) was kept in a pressure glass reaction tube at 75 °C for 24h. After cooling to room temperature, filtered and left in glove box at room temperature for three days to afford yellow block crystals in a yield of 33.6 mg (47.7%). Elemental analysis calcd (%) for $C_{57}H_{63}Br_3DyO_9P_3$: C, 49.35; H, 4.58. Found (%): C, 49.01; H, 4.86. IR (KBr, cm^{-1}): 3050(w), 2985(w), 2946(w), 2904(w), 1623(m), 1529(w), 1448(w), 1410(w), 1393(w), 1370(w), 1347(w), 1283(w), 1253(w), 1175(vs), 1051(vs), 1028(vs), 974(w), 929(w), 891(w), 819(w), 784(w), 735(m), 692(w), 641(w), 603(w), 571(w), 539(w), 502(w).

Crystallographic data collection and refinement

Single crystals of **α-DyCl**, **β-DyCl** and **β-DyBr** were used for data collection on a Bruker D8 Venture diffractometer using graphite monochromated Mo Kα ($λ$ = 0.71073 Å) radiation. The data were integrated using the Siemens SAINT program,[2] with the intensities corrected for the Lorentz factor, polarization, air absorption, and absorption due to variation in the path length through the detector faceplate. Empirical absorption and extinction corrections were applied using the SADABS program.[3] The structures were solved and refined on F^2 by full-matrix least squares using Olex2 (**α-DyCl** and **β-DyBr**) and SHELXTL(**β-DyCl**).[4,5] All the non-hydrogen atoms were refined anisotropically. The hydrogen atoms were refined with fixed isotropic displacement parameters. The residual electron densities were of no chemical significance. CCDC 2169008-2169010 contain the supplementary crystallographic data for this paper. These data can be obtained free of charge from the Cambridge Crystallographic Data Centre via

www.ccdc.cam.ac.uk/data_request/cif. Detailed crystal data and structural refinement parameters are listed in Table S1.
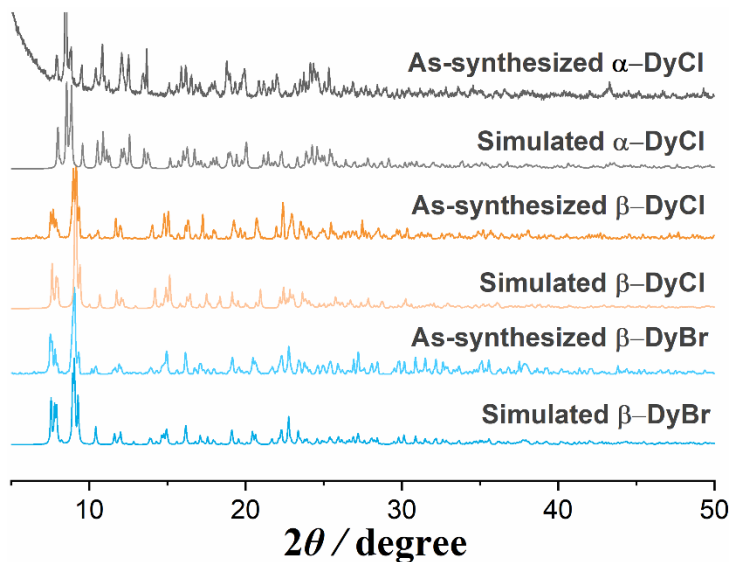
II. Primary characterization

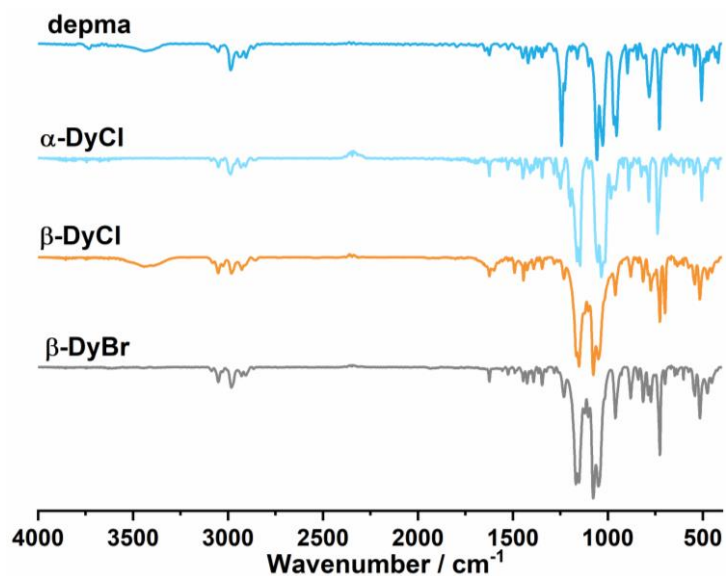**Figure S1.** Experimental and simulated PXRD patterns for complexes **α-DyCl**, **β-DyCl** and **β-DyBr**.

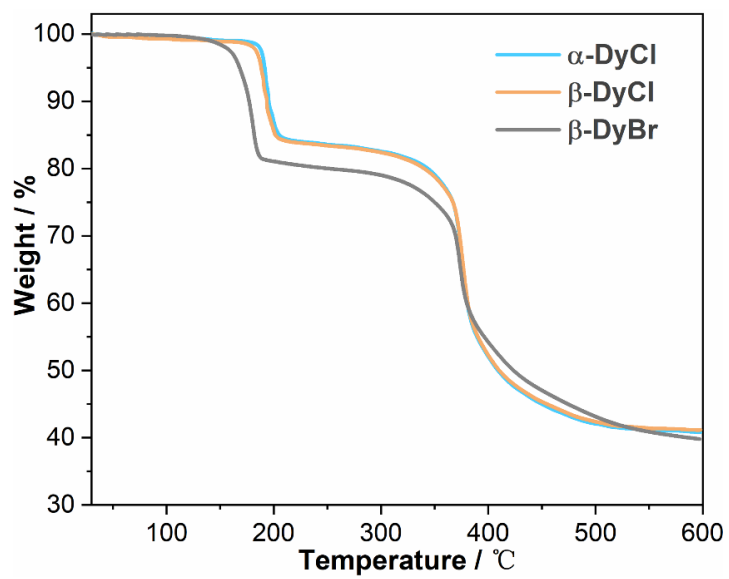

Figure S2. IR plots for **depma**, **α-DyCl**, **β-DyCl** and **β-DyBr**.

Figure S3. TG plots for complexes **α-DyCl**, **β-DyCl** and **β-DyBr**.

III. Crystal structures

Table S1. Crystal Data for complexes **α-DyCl**, **β-DyCl** and **β-DyBr**.

	α-DyCl	β-DyCl	β-DyBr
Empirical formula	$C_{57}H_{63}Cl_3DyO_9P_3$	$C_{57}H_{63}Cl_3DyO_9P_3$	$C_{57}H_{63}Br_3DyO_9P_3$
Formula weight	1253.83	1253.83	1387.21
Crystal system	triclinic	triclinic	triclinic
Space group	P-1	P-1	P-1
a (Å)	11.048(1)	10.688(1)	10.876(4)
b (Å)	11.370(1)	11.871(1)	12.003(5)
c (Å)	22.337(1)	22.785(1)	23.079(9)
α (°)	89.823(2)	79.887(2)	80.018(6)
β (°)	81.860(2)	86.071(2)	85.631(7)
γ (°)	82.276(2)	81.983(2)	80.695(6)
V (Å^3)	2752.2(4)	2815.2(3)	2924.9(1)
Z	2	2	2
μ (mm^{-1})	1.646	1.609	3.461
Unique reflections	12492	12709	10339
Observed reflections	25820	25350	22574
R_{int}	0.0489	0.0374	0.0503
Final R indices	$R_1 = 0.0370$	$R_1 = 0.0449$	$R_1 = 0.0441$
[$I > 2\sigma(I)$][a]	$wR_2 = 0.0866$	$wR_2 = 0.1111$	$wR_2 = 0.1110$
R indices (all data) [a]	$R_1 = 0.0452$	$R_1 = 0.0490$	$R_1 = 0.0760$
	$wR_2 = 0.0924$	$wR_2 = 0.1148$	$wR_2 = 0.1251$
CCDC number	2169008	2169009	2169010

[a] $R_1 = \Sigma||F_o| - |F_c||/\Sigma|F_o|$. $wR_2 = [\Sigma w(F_o^2 - F_c^2)^2/\Sigma w(F_o^2)^2]^{1/2}$

Table S2. Continuous Shape Measure (CShM) analyses of dysprosium geometries for **α-DyCl**, **β-DyCl** and **β-DyBr** using the SHAPE2.1 Software.

Geometry	α-DyCl	β-DyCl	β-DyBr
Hexagon(D_{6h})	30.012	32.355	32.351
Pentagonal pyramid(C_{5v})	26.851	27.291	27.411
Octahedron (O_h)	0.808	0.846	1.295
Trigonal prism (D_{3h})	15.642	15.265	15.810
Johnson pentagonal pyramid J2 (C_{5v})	29.744	30.137	29.969

Table S3. Selected bond lengths (Å) and bond angles (°) for complexes **α-DyCl**, **β-DyCl** and **β-DyBr**.

α-DyCl			
Dy1-O1	2.300(2)	O4-Dy1-Cl3	94.11(7)
Dy1-O4	2.262(2)	O4-Dy1-O1	90.04(8)
Dy1-O7	2.289(2)	O4-Dy1-O7	175.97(8)
Dy1-Cl1	2.608(1)	O7-Dy1-Cl1	89.66(6)
Dy1-Cl2	2.625(1)	O7-Dy1-Cl2	94.53(6)
Dy1-Cl3	2.612(1)	O7-Dy1-Cl3	89.54(6)
O1-Dy1-Cl1	90.03(6)	O7-Dy1-O1	86.32(8)
O1-Dy1-Cl2	85.68(6)	Cl1-Dy1-Cl2	173.79(3)
O1-Dy1-Cl3	175.84(6)	Cl1-Dy1-Cl3	89.52(3)
O4-Dy1-Cl1	92.06(6)	Cl2-Dy1-Cl3	95.08(3)
O4-Dy1-Cl2	83.47(6)		
β-DyCl			
Dy1-O1	2.288(3)	O4-Dy1-Cl3	88.00(7)
Dy1-O4	2.265(3)	O4-Dy1-O1	89.42(10)
Dy1-O7	2.258(3)	O7-Dy1-Cl1	89.54(8)
Dy1-Cl1	2.611(1)	O7-Dy1-Cl2	91.04(8)
Dy1-Cl2	2.644(1)	O7-Dy1-Cl3	93.29(7)
Dy1-Cl3	2.617(1)	O7-Dy1-O1	89.30(10)
O1-Dy1-Cl1	85.35(9)	O7-Dy1-O4	177.67(11)
O1-Dy1-Cl2	84.03(8)	Cl1-Dy1-Cl2	169.36(4)
O1-Dy1-Cl3	177.40(8)	Cl1-Dy1-Cl3	94.39(4)
O4-Dy1-Cl1	92.30(8)	Cl2-Dy1-Cl3	96.18(3)
O4-Dy1-Cl2	86.89(8)		
β-DyBr			
Dy1-O1	2.284(4)	O4-Dy1-Br3	88.26(9)
Dy1-O4	2.268(4)	O4-Dy1-O1	90.74(13)
Dy1-O7	2.250(4)	O7-Dy1-Br1	91.53(11)
Dy1-Br1	2.784 (1)	O7-Dy1-Br2	90.64(11)
Dy1-Br2	2.760 (1)	O7-Dy1-Br3	92.50(10)
Dy1-Br3	2.759(1)	O7-Dy1-O1	88.48(14)
O1-Dy1-Br1	83.53(10)	O7-Dy1-O4	177.78(14)
O1-Dy1-Br2	86.52(10)	Br1-Dy1-Br2	169.76(2)
O1-Dy1-Br3	178.72(9)	Br1-Dy1-Br3	95.60(3)
O4-Dy1-Br1	86.32(10)	Br2-Dy1-Br3	94.30(3)
O4-Dy1-Br2	91.38(10)		

Table S4. The parameters of H-bonding for **α-DyCl**, **β-DyCl** and **β-DyBr**.

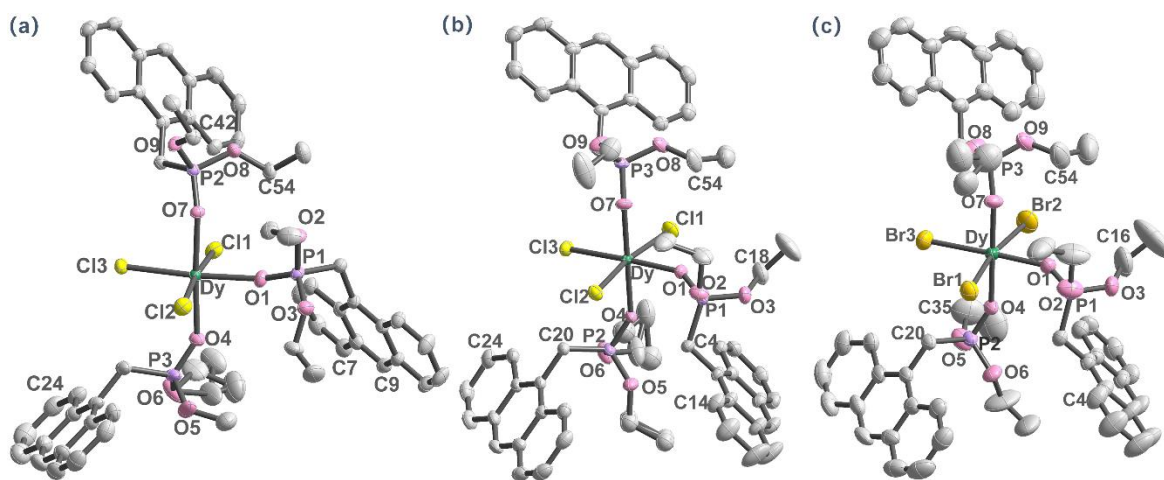| Complex	D-H···A	dD···A (Å)	dH···A (Å)	∠D-H···A (°)
	C9-H9···Cl2(inter)	3.645(4)	2.715(4)	178.45(4)
	C7-H7···Cl3(inter)	3.606(4)	2.781(4)	148.37(4)
	C24-H24···Cl2(inter)	3.604(4)	2.871(4)	136.55(4)
α-DyCl	C42-H42···Cl1 (intra)	3.614(4)	2.719(4)	161.63(3)
	C37-H37A···O2(intra)	3.000(4)	2.542(4)	108.91(3)
	C56-H56B···π(inter)	3.711(3)	2.963(3)	134.8(3)
	C57-H57C···π(inter)	3.927(4)	3.141(16)	140.1(9)
	C14-H14···π (inter)	3.628(4)	2.846(4)	140.29(4)
β-DyCl	C24-H24···O2(inter)	3.267(5)	2.688(5)	120.01(4)
	C54-H54A···O7(intra)	3.020(7)	2.548(7)	109.14(6)
	C4-H4···O4(intra)	3.415(5)	2.625(5)	140.82(4)
	C18-H18A···O1(intra)	2.927(7)	2.428(2)	110.61(6)
	C20-H20A···Cl2(intra)	3.646(4)	2.836(4)	139.58(3)
	C20-H20B···Cl3(intra)	3.671(4)	2.912 (4)	134.16(3)
	C4-H4···π(inter)	3.722(5)	2.959(9)	140.25(3)
	C35-H56A···O2(inter)	3.632(1)	2.667(5)	174.00(7)
	C54-H54A···O7(intra)	3.026(9)	2.567(4)	109.08(5)
β-DyBr	C16-H16A···O1(intra)	2.919(1)	2.423(3)	111.29(5)
	C20-H20B···Br1(intra)	3.759(6)	2.992(1)	136.94(3)
	C1-H1A···O8(intra)	3.216(7)	2.824(3)	106.61(4)
	C35-H35B···O4(intra)	2.994(1)	2.529(4)	109.36(7)

Figure S4. Structure of complexes **α-DyCl**, **β-DyCl** and **β-DyBr** with an atomic labelling scheme (50% probability).
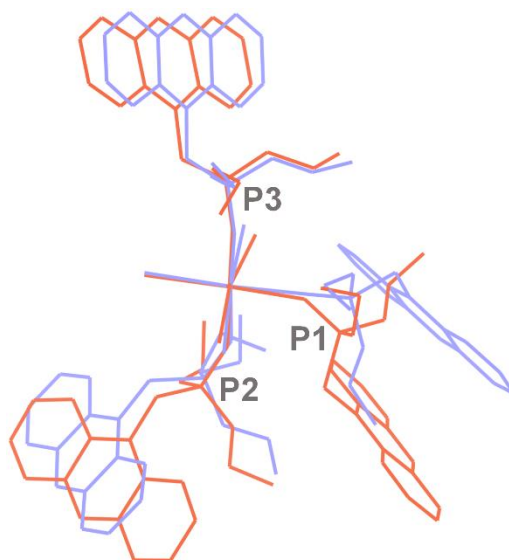

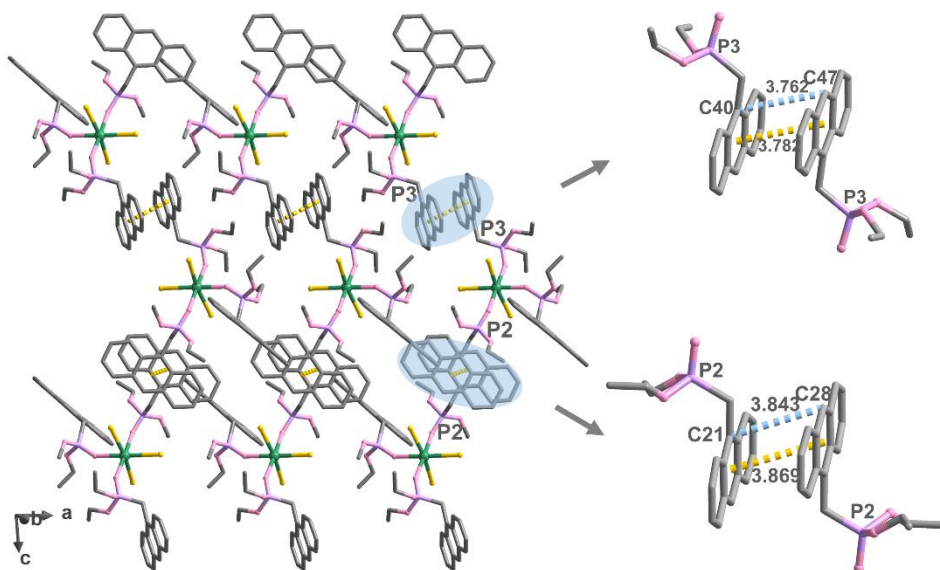**Figure S5.** Overlay of the molecular structures of complexes **α-DyCl** (purple) and **β-DyCl** (red).

Figure S6. Packing diagrams viewed along the *b* axis of **β-DyBr**. The shaded circles depict the face-to-face π⋯π interactions. All hydrogen atoms are omitted for clarity.
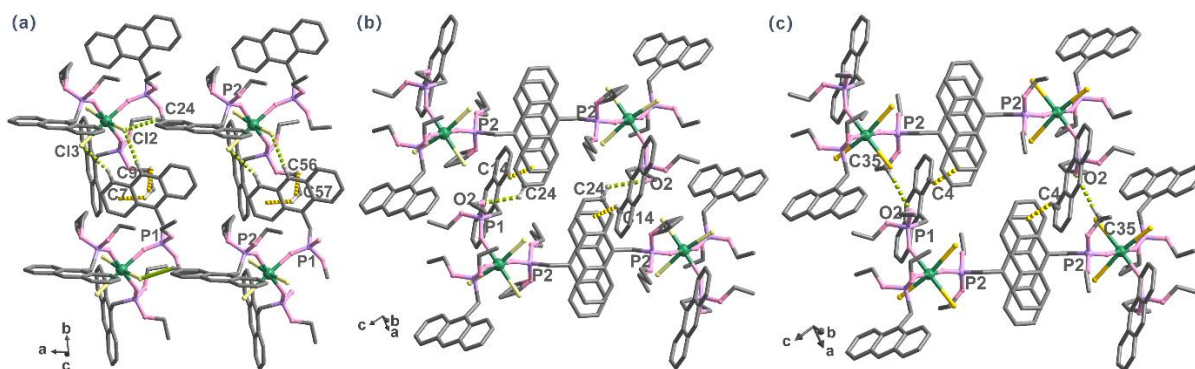

Figure S7 The intermolecular H-bond interactions of C-H⋯π (yellow) and C-H⋯O/Cl/Br (green) among the molecules of **α-DyCl** (a), **β-DyCl** (b) and **β-DyBr** (c). Some hydrogen atoms are omitted for clarity.

IV. Magnetic studies

Table S5. The fit parameters obtained from analyses of the ac susceptibilities of **α-DyCl** under 1 kOe bias dc field.

T / K	χ_T / cm^3 mol^{-1}	χ_S / cm^3 mol^{-1}	$\ln(\tau / s)$	α	Residual
2	2.13	0.20	-5.97	0.28	4.21×10^{-2}
2.2	2.02	0.23	-6.31	0.30	5.60×10^{-2}
2.4	1.83	0.29	-6.80	0.27	3.58×10^{-2}
2.6	1.71	0.37	-7.28	0.26	1.95×10^{-2}
2.8	1.60	0.48	-7.77	0.26	6.57×10^{-2}
3	1.52	0.61	-8.26	0.27	2.42×10^{-2}
3.3	1.38	0.81	-9.08	0.25	2.46×10^{-2}
3.7	1.24	1.01	-10.07	0.23	2.20×10^{-2}
4.1	1.13	1.04	-11.26	0.28	1.71×10^{-2}

Table S6. The fit parameters obtained from analyses of the ac susceptibilities of **β-DyCl** under 1 kOe bias dc field.

T / K	χ_T / cm^3 mol^{-1}	χ_S / cm^3 mol^{-1}	$\ln(\tau / s)$	α	Residual
2	2.79	0.09	-2.92	0.23	2.54×10^{-2}
2.2	2.51	0.09	-3.30	0.21	1.40×10^{-2}
2.4	2.28	0.09	-3.70	0.19	1.98×10^{-2}
2.6	2.10	0.08	-4.11	0.20	2.95×10^{-2}
2.8	1.92	0.10	-4.57	0.17	2.42×10^{-2}
3	1.80	0.10	-4.93	0.16	1.83×10^{-2}
3.3	1.62	0.11	-5.51	0.13	1.77×10^{-2}
3.7	1.46	0.11	-6.21	0.11	1.33×10^{-2}
4.1	1.31	0.12	-6.86	0.07	5.95×10^{-3}
4.5	1.19	0.12	-7.48	0.05	2.88×10^{-3}
5	1.08	0.13	-8.21	0.04	3.62×10^{-3}
5.5	0.98	0.07	-9.09	0.05	5.52×10^{-3}
6	0.91	1.72	-9.99	0.03	4.31×10^{-3}

Table S7. The fit parameters obtained from analyses of the ac susceptibilities of **β-DyBr** under 1 kOe bias dc field.

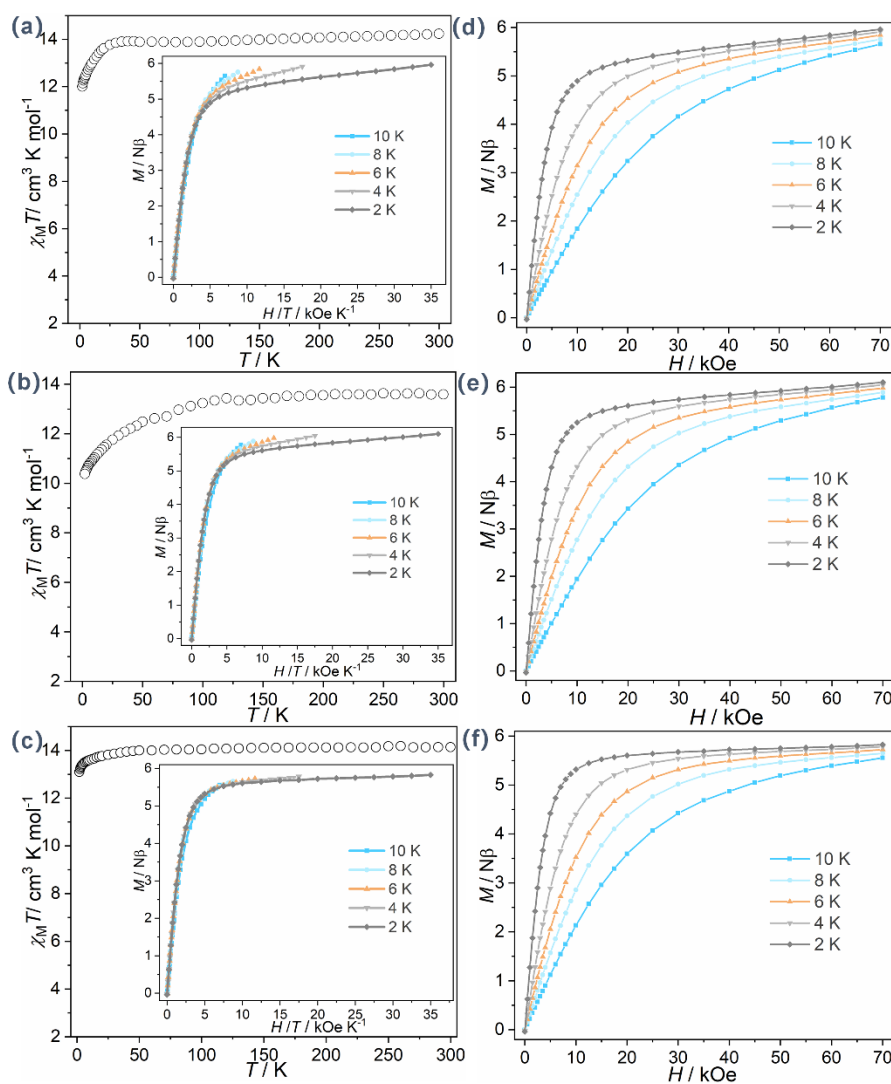| T / K	χ_T / cm^3 mol^{-1}	χ_S / cm^3 mol^{-1}	$\ln(\tau / s)$	α	Residual
2	3.69	0.09	-1.93	0.41	1.04×10^{-2}
2.2	3.33	0.08	-2.17	0.40	1.27×10^{-2}
2.4	3.00	0.08	-2.34	0.40	5.68×10^{-3}
2.6	2.73	0.09	-2.69	0.38	8.17×10^{-3}
2.8	2.43	0.09	-2.95	0.36	1.29×10^{-2}
3	2.31	0.09	-3.17	0.37	6.73×10^{-3}
3.3	2.10	0.08	-3.46	0.39	1.08×10^{-2}
3.7	1.88	0.07	-3.8	0.40	2.25×10^{-2}
4.1	1.69	0.08	-4.11	0.34	3.11×10^{-2}
4.5	1.50	0.11	-4.39	0.24	3.57×10^{-2}
5	1.29	0.16	-4.76	0.25	2.67×10^{-2}
5.5	1.16	0.23	-5.12	0.16	1.48×10^{-2}
6	1.05	0.25	-5.59	0.09	7.15×10^{-3}
7	0.89	0.26	-6.42	0.06	1.05×10^{-3}
8	0.78	0.23	-7.19	0.04	2.32×10^{-2}
9	0.70	0.21	-7.86	0.04	5.75×10^{-2}
10	0.64	0.19	-8.51	0.06	3.87×10^{-2}
12	0.52	0.16	-10.01	0.08	7.58×10^{-4}

Figure S8. (a-c) Plots of $\chi_M T$ vs T for **α-DyCl** (a), **β-DyCl** (b) and **β-DyBr** (c). Inset: Plots of M vs H/T at different temperatures; (d-f) Field dependence of the magnetization at depicted temperatures for **α-DyCl** (d), **β-DyCl** (e) and **β-DyBr** (f).
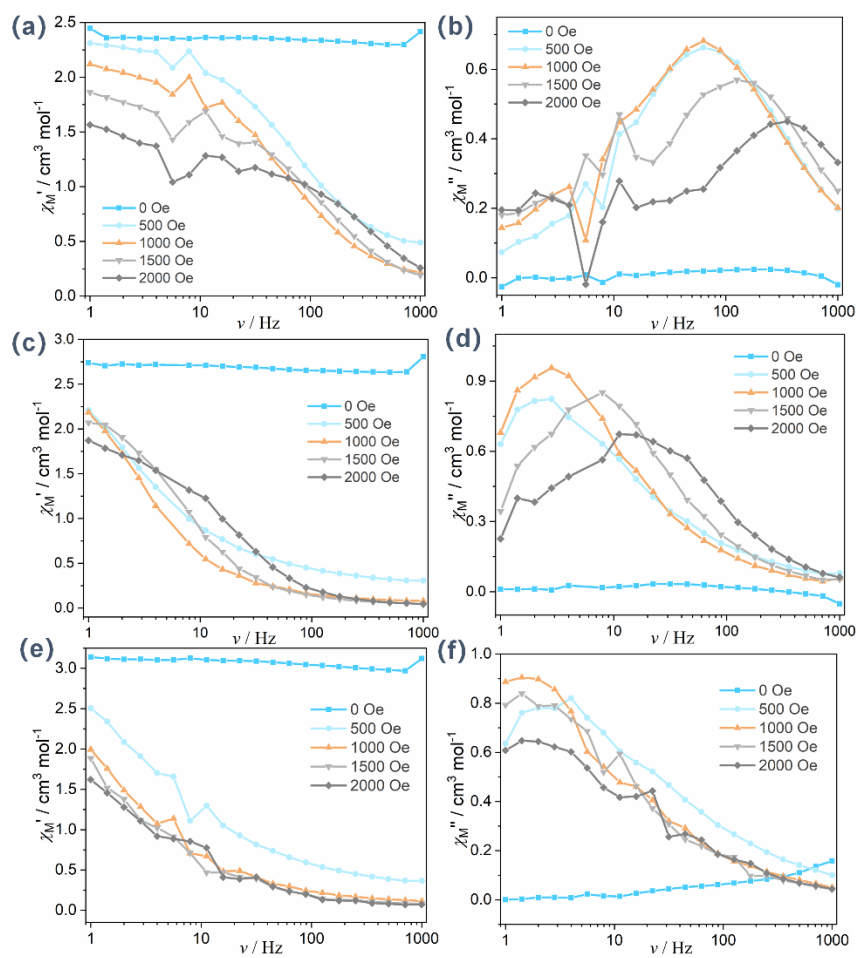
Figure S9. In-phase (χ') and out-of-phase (χ'') ac susceptibilities at depicted dc field for **α-DyCl** (a, b), **β-DyCl** (c, d) and **β-DyBr** (e, f)

.

Figure S10. (a-c) Frequency dependent in-phase (χ') signals of ac susceptibilities for complexes **α-DyCl** (a), **β-DyCl** (b) and **β-DyBr** (c) measured under 1 kOe dc field; (d-f) Cole-Cole plots for **α-DyCl** (d), **β-DyCl** (e) and **β-DyBr** (f) measured in the different temperatures range under 1 kOe Oe dc field. The solid line represents the best fit using a generalized Debye model.

V. Magnetic computational details

Complete-active-space self-consistent field (CASSCF) calculations on mononuclear complexes **α-DyCl**, **β-DyCl** and **β-DyBr** (see Figure S1 for the calculated complete structures of **α-DyCl**, **β-DyCl** and **β-DyBr**) on the basis of single-crystal X-ray determined geometries have been carried out with OpenMolcas[5] program package.

The basis sets for all atoms are atomic natural orbitals from the OpenMolcas ANO-RCC library: ANO-RCC-VTZP for Dy^{III}; VTZ for close Cl, Br and O; VDZ for distant atoms. The calculations employed the second order Douglas-Kroll-Hess Hamiltonian, where scalar relativistic contractions were taken into account in the basis set and the spin-orbit couplings were handled separately in the restricted active space state interaction (RASSI-SO) procedure. For complexes **α-DyCl**, **β-DyCl** and **β-DyBr**, active electrons in 7 active orbitals include all *f* electrons (CAS (9 in 7 for Dy^{III}) in the CASSCF calculation. To exclude all the doubts, we calculated all the roots in the active space. We have mixed the maximum number of spin-free state which was possible with our hardware (all from 21 sextets, 128 from 224 quadruplets, 130 from 490 doublets for Dy^{III}). SINGLE_ANISO[6–8] program was used to obtain the energy levels, *g* tensors, magnetic axes, et al. based on the above CASSCF/RASSI-SO calculations.
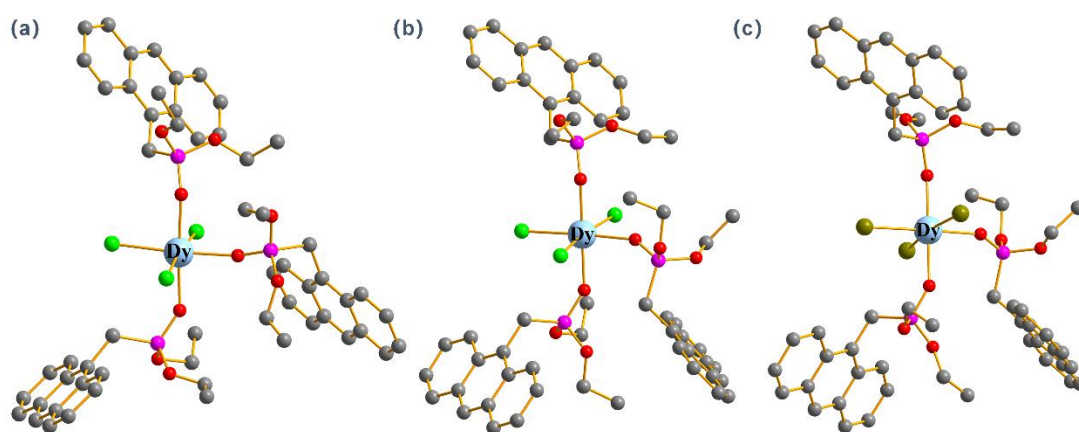

Figure S11. Calculated complete structures of complexes **α-DyCl** (a), **β-DyCl** (b) and **β-DyBr** (c); H atoms are omitted for clarify.

Table S8. Calculated energy levels (cm^{-1}), g (g_x, g_y, g_z) tensors and predominant m_J values of the lowest eight Kramers doublets (KDs) of complexes **α-DyCl**, **β-DyCl** and **β-DyBr** using CASSCF/RASSI-SO with OpenMolcas.

KDs	α-DyCl			β-DyCl			β-DyBr		
	E/cm^{-1}	g	m_J	E/cm^{-1}	g	m_J	E/cm^{-1}	g	m_J
1	0.0	0.939 4.002 13.924	±15/2	0.0	0.113 0.449 19.069	±15/2	0.0	0.006 0.058 19.676	±15/2
2	21.4	0.541 4.760 11.852	±9/2	57.2	0.737 6.465 13.314	±1/2	100.4	0.617 0.804 18.894	±1/2
3	51.0	0.485 2.280 11.747	±9/2	83.4	0.758 5.522 10.852	±3/2	167.3	1.954 4.480 12.956	±13/2
4	138.5	5.942 6.323 9.032	±7/2	158.6	5.382 6.572 9.643	±13/2	197.0	8.978 6.542 2.129	±3/2
5	227.0	0.643 1.126 16.861	±11/2	283.1	3.095 3.510 7.735	±5/2	311.9	7.194 5.782 4.118	±5/2
6	286.2	3.274 4.747 10.013	±13/2	322.3	2.438 3.357 11.419	±7/2	357.9	0.459 4.836 11.155	±11/2
7	330.0	10.416 7.044 2.083	±7/2	342.7	10.462 7.028 2.820	±11/2	375.4	10.892 6.908 2.604	±7/2
8	398.9	0.307 1.087 17.614	±1/2	402.5	0.488 1.128 17.204	±9/2	431.3	0.130 1.102 17.265	±9/2

Table S9. Wave functions with definite projection of the total moment | m_J > for the lowest eight KDs of complexes **α-DyCl**, **β-DyCl** and **β-DyBr**.

	E/cm^{-1}	wave functions
α-DyCl	0.0	39.4%|±15/2>+29.6%|±11/2>+13.0%|±7/2>+5.4%|±5/2>+4.7%|±13/2>
	21.4	19.9%|±9/2>+19.4%|±13/2>+16.5%|±7/2>+13.3%|±5/2>+12.4%|±15/2>+7.9%|±3/2>
	51.0	23.5%|±9/2>+21.2%|±3/2>+20.1%|±1/2>+16.2%|±5/2>+14.3%|±13/2>
	138.5	31.2%|±7/2>+20.5%|±15/2>+12.8%|±5/2>+11.2%|±9/2>+11.0%|±3/2>+5.8%|±13/2>
	227.0	35.0%|±11/2>+22.7%|±13/2>+18.6%|±15/2>+8.0%|±9/2>+7.3%|±5/2>
	286.2	25.2%|±13/2>+15.9%|±9/2>+15.4%|±5/2>+15.2%|±1/2>+10.6%|±11/2>+8.4%|±7/2>
	330.0	21.6%|±7/2>+17.2%|±3/2>+13.9%|±9/2>+13.1%|±11/2>+11.8%|±5/2>
	398.9	37.1%|±1/2>+30.4%|±3/2>+17.7%|±5/2>+5.8%|±7/2>
β-DyCl	0.0	94.2%|±15/2>
	57.2	79%|±1/2>+9.1%|±3/2>+4.4%|±9/2>
	83.4	51.9%|±3/2>+24.5%|±5/2>+9.5%|±13/2>+6%|±11/2>
	158.6	56.2%|±13/2>+21.0%|±3/2>+13.1%|±5/2>
	283.1	48.7%|±5/2>+31.3%|±13/2>+7.5%|±11/2>+6.9%|±7/2>
	322.3	54.1%|±7/2>+24.2%|±9/2>+12.7%|±11/2>
	342.7	58.2%|±11/2>+13.3%|±9/2>+11%|±3/2>+8.3%|±7/2>
	402.5	55.2%|±9/2>+20.6%|±7/2>+10.9%|±11/2>+6.0%|±1/2>
β-DyBr	0.0	98.3%|±15/2>
	100.4	51.6%|±1/2>+24.5%|±3/2>+11.1%|±5/2>+4.1%|±7/2>
	167.3	62.6%|±13/2>+16.7%|±1/2>+13.2%|±5/2>
	197.0	49.2%|±3/2>+19.4%|±1/2>+15.7%|±13/2>+12.0%|±11/2>
	311.9	54.0%|±5/2>+16.1%|±13/2>+14.5%|±7/2>+8.6%|±11/2>
	357.9	66.9%|±11/2>+11.3%|±3/2>+10.1%|±9/2>+6.6%|±7/2>
	375.4	47.2%|±7/2>+28.5%|±9/2>+11.4%|±5/2>+5.9%|±3/2>
	431.3	51.2%|±9/2>+24.2%|±7/2>+7.99%|±11/2>+6.8%|±5/2>

Figure S12. Magnetization blocking barriers of complexes **α-DyCl** (a), **β-DyCl** (b) and **β-DyBr** (c). The thick black lines represent the KDs as a function of their magnetic moment along the magnetic axis. The green lines correspond to diagonal quantum tunneling of magnetization (QTM); the blue line represent off-diagonal relaxation process. The path shown by the red arrows represents the most probable path for magnetic relaxation in the corresponding complexes. The numbers at each arrow stand for the mean absolute value of the corresponding matrix element of transition magnetic moment.

Recently, Aravena *et al.* [9–10] proposed a method for the prediction of tunneling demagnetization time (τ_{QTM}), we calculated the value of τ_{QTM} according to equations (S1)–(S2).

$$\tau_{QTM} = \frac{1}{2k} \qquad\qquad (S1)$$

$$k = \frac{\beta B_{ave}}{h} \cdot \frac{g_{XY}^2}{2(g_{XY}^2 + g_Z^2)^{\frac{1}{2}}} \qquad\qquad (S2)$$

Where $g_{XY}^2 = (g_X^2 + g_Y^2)$, k is the rate of ground state QTM. Usually, the magnitude of the magnetic fields, arising from both dipolar and hyperfine interactions, is of a few tens of mini-Tesla (mT). Thus, in this work, B_{ave} is set to be 20 mT.

The relevant parameters and the values of τ_{QTM} are shown in Table S10, where the calculated τ_{QTM} of **α-DyCl**, **β-DyCl** and **β-DyBr** are 3.07×10^{-9}, 3.18×10^{-7} and 2.06×10^{-5} s, respectively. The very small τ_{QTM} of complex **α-DyCl** leads to the absence of energy barrier. The calculated crystal-field (CF) parameters B (k, q) with high percentage of **α-DyCl**, **β-DyCl** and **β-DyBr** are shown in Table S11. The weights of the axial parameters B (2, 0) for **α-DyCl**, **β-DyCl** and **β-DyBr** are 5.59 %, 5.08 % and 9.98%, respectively, slightly higher than other nonaxial CF parameters B (2, q), which shows that the axial symmetries of **α-DyCl**, **β-DyCl** and **β-DyBr** are not very high. Among three complexes, the axial symmetry of complex **β-DyBr** is the highest.

Table S10. Values of B_{ave}, principal values of the g-tensor of the lowest KD and the QTM time (τ_{QTM}).

Complex	B_{ave} (mT)	g_X	g_Y	g_Z	τ_{QTM} (s)
α-DyCl	20	9.3951×10^{-1}	4.0024	13.9249	3.07×10^{-9}
β-DyCl	20	1.1302×10^{-1}	4.4920×10^{-1}	19.0699	3.18×10^{-7}
β-DyBr	20	6.4203×10^{-3}	5.8124×10^{-2}	19.6767	2.06×10^{-5}

Table S11. Weight of calculated crystal-field parameters B(k,q) of complexes **α-DyCl**, **β-DyCl** and **β-DyBr**.

k	*q*	**α-DyCl**	**β-DyCl**	**β-DyBr**
	−2	4.93%	3.77%	0.06%
	−1	3.68%	3.94%	2.09%
2	0	5.59%	5.08%	9.98%
	1	2.49%	3.27%	3.74%
	2	1.38%	0.26%	8.40%
	−4	11.40%	4.30%	11.90%
	−3	0.73%	3.31%	2.29%
	−2	12.04%	0.91%	0.25%
	−1	11.08%	4.61%	2.11%
4	0	0.63%	20.82%	18.86%
	1	1.99%	3.41%	2.69%
	2	15.49%	1.64%	2.61%
	3	2.58%	0.96%	0.77%
	4	0.31%	19.09%	11.18%
	−6	1.78%	1.38%	1.32%
	−5	0.13%	0.97%	0.26%
	−4	2.22%	1.66%	4.67%
	−3	1.50%	2.07%	1.42%
	−2	0.47%	0.25%	0.34%
	−1	2.84%	0.11%	0.38%
6	0	3.02%	4.65%	4.45%
	1	2.08%	0.51%	0.35%
	2	0.99%	1.08%	1.14%
	3	2.41%	0.73%	0.34%
	4	1.27%	7.26%	4.42%
	5	1.74%	0.83%	0.69%
	6	2.33%	1.11%	1.57%

The program POLY_ANISO[6-8] was used to fit the magnetic susceptibilities of complexes **α-DyCl**, **β-DyCl** and **β-DyBr**. The intermolecular interactions zJ' of **α-DyCl**, **β-DyCl** and **β-DyBr** were fitted to 0.05, −0.03 and 0.0007 cm^{-1}, respectively. The calculated and experimental $\chi_M T$ versus T plots of complexes **α-DyCl**, **β-DyCl** and **β-DyBr** were shown in Figure S3, where only the fit of **β-DyCl** is close to the experiment in the whole temperature. The main magnetic axes on Dy^{III} ions of **α-**

DyCl, **β-DyCl** and **β-DyBr** in their ground KDs are indicated in Figure S4, and all of which lie almost along the O–Dy–O direction.
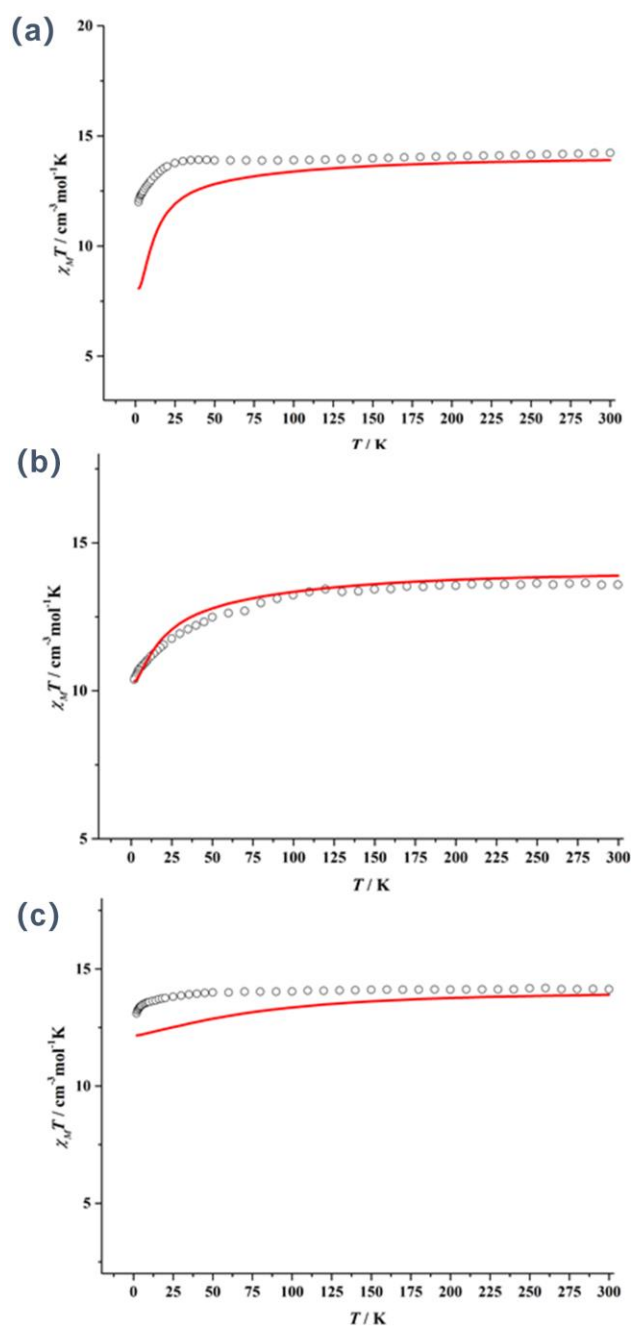

Figure S13. Calculated (red solid line) and experimental (white circle) data of magnetic susceptibility of complexes **α-DyCl**, **β-DyCl** and **β-DyBr**. The intermolecular interaction zJ' of **α-DyCl**, **β-DyCl** and **β-DyBr** were fitted to 0.05, –0.03 and 0.0007 cm^{-1}, respectively.
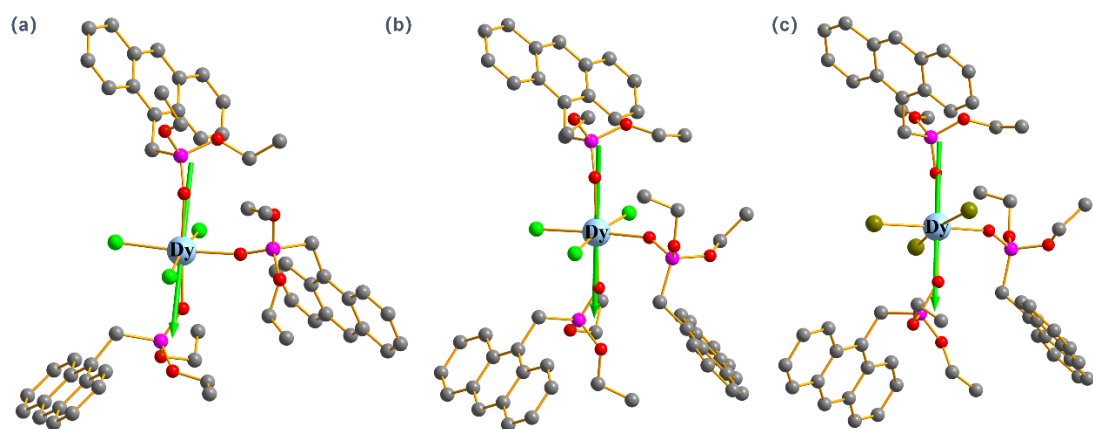
Figure S14. Calculated orientations of the local main magnetic axes on Dy^{III} ions of complexes **α-DyCl** (a), **β-DyCl** (b) and **β-DyBr** (c) in the ground KDs.

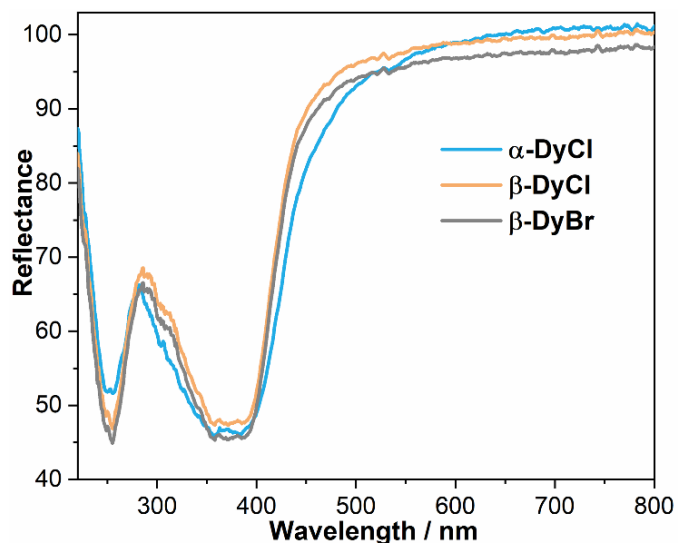# VI. Photoluminescent properties

Figure S15. The UV-vis reflectance spectra for complexes **α-DyCl**, **β-DyCl** and **β-DyBr**.
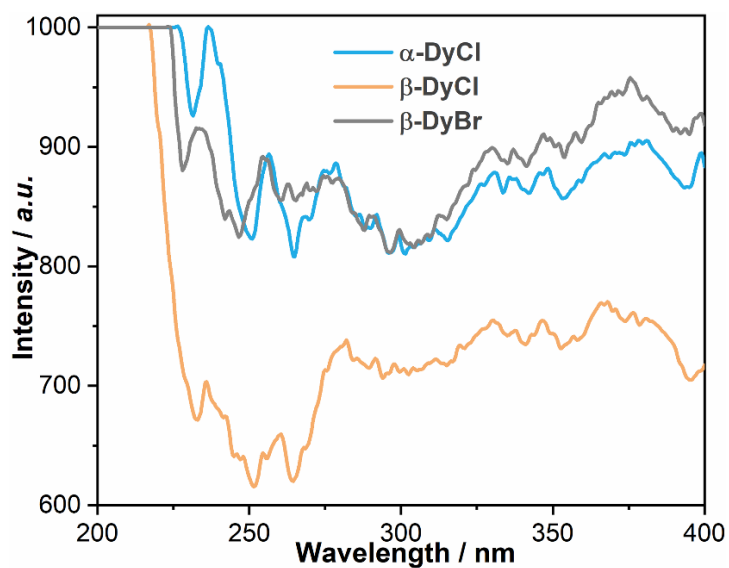

Figure S16. The excitation (200-400 nm) spectra monitored at emission wavelength λ_{em} = 487 nm for **α-DyCl** and λ_{em} = 535 nm for **β-DyCl** and **β-DyBr**.
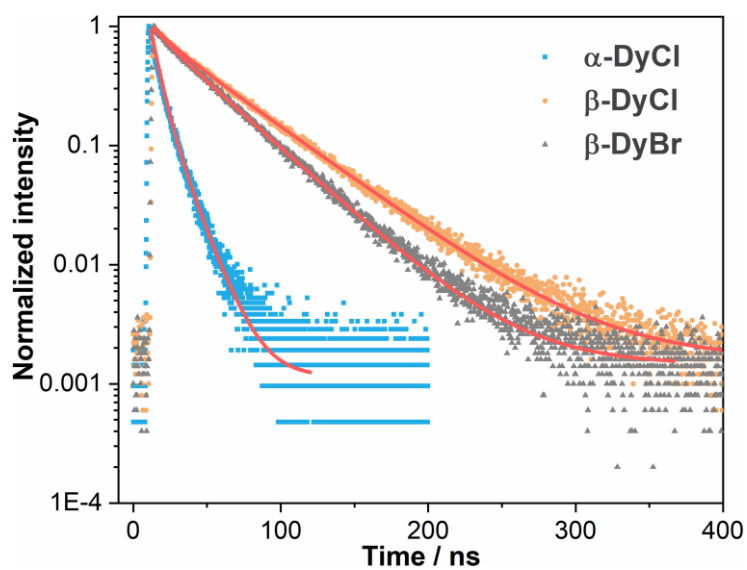
Figure S17. Fluorescence decay curve for **α-DyCl**, **β-DyCl** and **β-DyBr** emitting at 487 nm, 530 nm and 530 nm (excited at 300 nm).

Table S12. The transient luminescent lifetime (τ) and absolute quantum yields (QY) at room temperature and the magnetic parameters for **α-DyCl**, **β-DyCl** and **β-DyBr**.

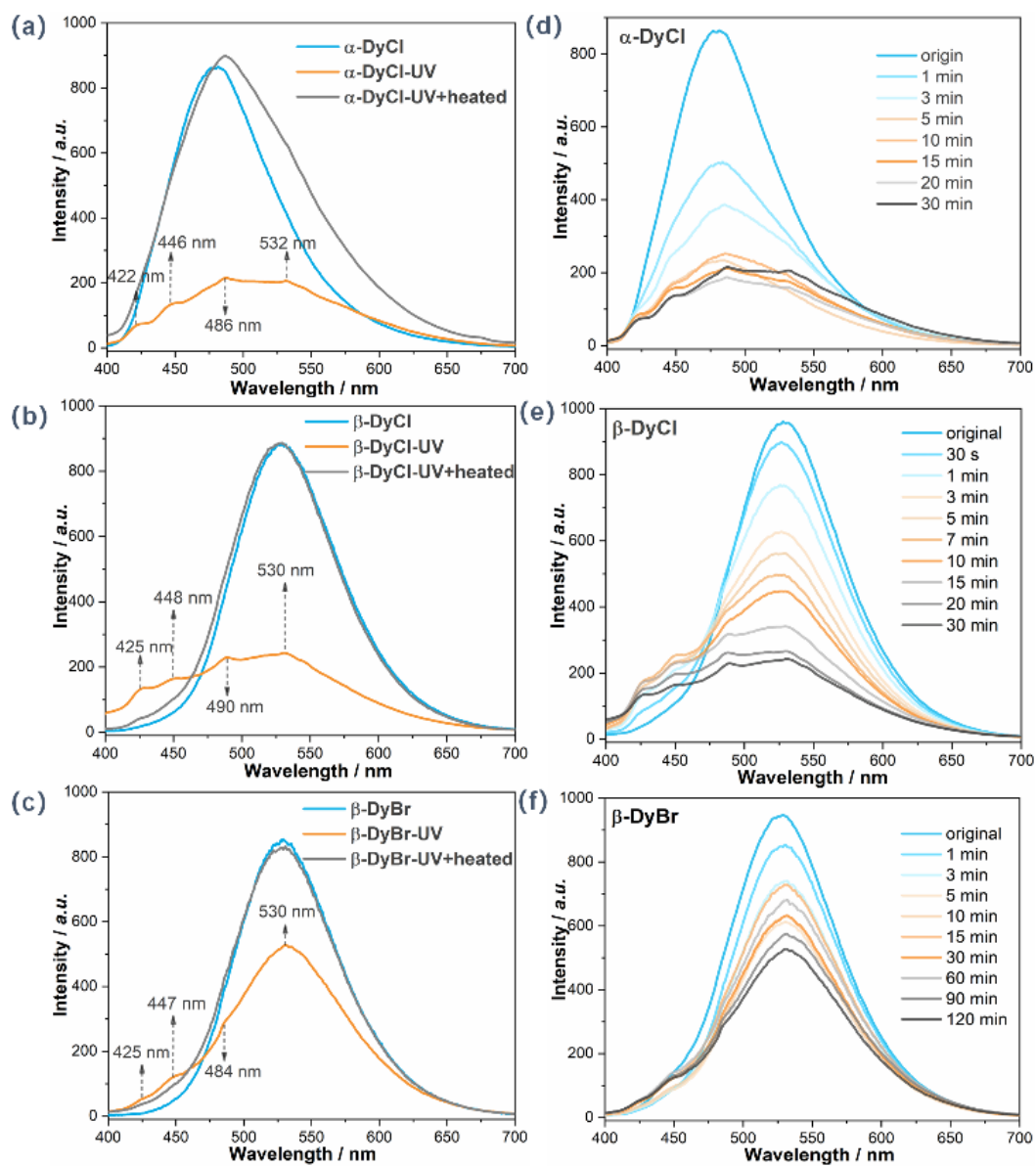| Complex	α-DyCl	β-DyCl	β-DyBr
λ_{em} / nm	487	530	530
τ / ns	10.8	48.6	38.8
χ^2	1.18	1.09	1.11
QY / %	23.17	43.61	24.95

Figure S18. The luminescence spectra for **α-DyCl** (a,d), **β-DyCl** (b,e) and **β-DyBr** (c,f) excited at 330 nm as a function of irradiation time by a 365 nm LED light.
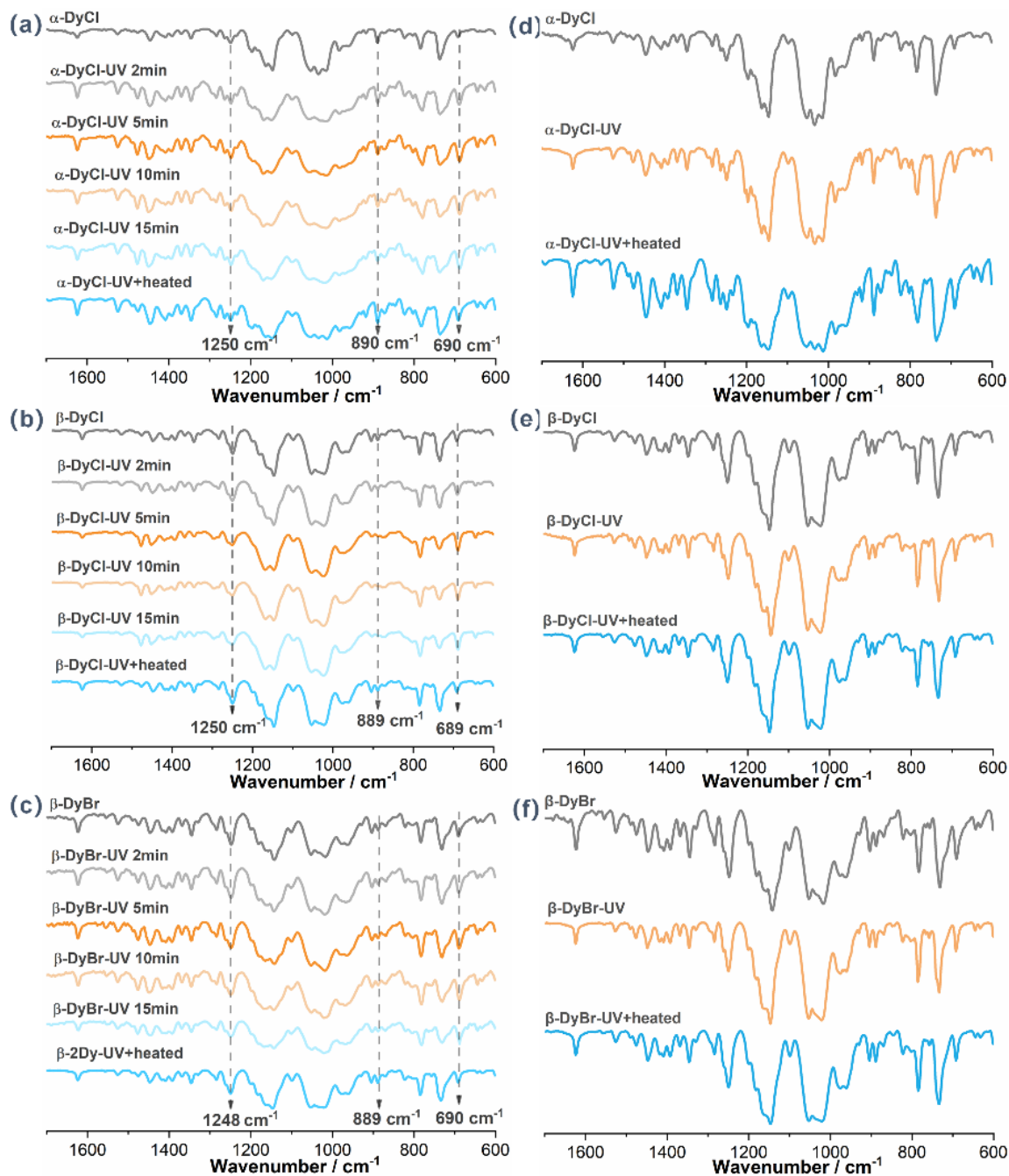
Figure S19. (a-c) The FTIR spectra for **α-DyCl** (a), **β-DyCl** (b) and **β-DyBr** (c) under different UV irradiation time. The grey dotted line highlight shows the changes possibly caused by photodimerization; (d-f) The FTIR spectra for **α-DyCl** (d), **β-DyCl** (e) and **β-DyBr** (f) under different conditions.
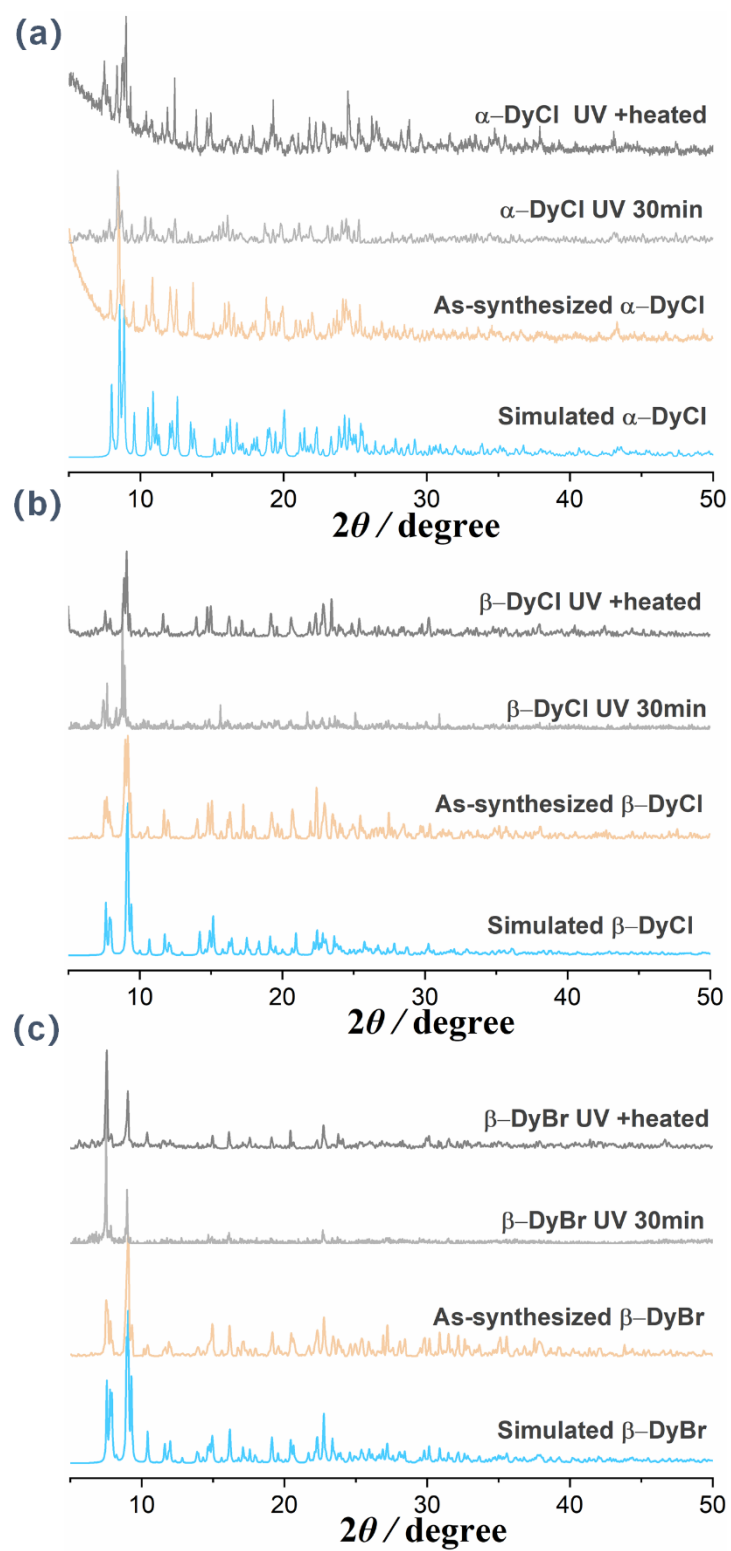
Figure S20. The PXRD patterns for **α-DyCl** (a), **β-DyCl** (b) and **β-DyBr** (c) under different conditions.

Table S13. Crystal Data for complexes **α-DyCl-UV** and **β-DyCl-UV**.

	α-DyCl-UV	β-DyCl-UV
Empirical formula	$C_{57}H_{63}Cl_3DyO_9P_3$	$C_{57}H_{63}Cl_3DyO_9P_3$
Formula weight	1253.83	1253.83
Crystal system	triclinic	triclinic
Space group	*P*-1	*P*-1
a (Å)	11.064(1)	10.757(1)
b (Å)	11.376(1)	11.857(1)
c (Å)	22.381(1)	22.848(2)
$α$ (°)	89.938(1)	79.999(3)
$β$ (°)	81.885(1)	85.745(3)
$γ$ (°)	82.236(1)	81.613(3)
V ($Å^3$)	2752.2(4)	2835.7(5)
Z	2	2
$μ$ (mm^{-1})	1.640	1.598
Unique reflections	11884	11858
Observed reflections	22770	20491
R_{int}	0.0384	0.0546
Final *R* indices	$R_1 = 0.0553$	$R_1 = 0.0965$
[$I > 2σ(I)$][a]	$wR_2 = 0.1812$	$wR_2 = 0.2877$
R indices (all data) [a]	$R_1 = 0.0620$	$R_1 = 0.1034$
	$wR_2 = 0.1945$	$wR_2 = 0.3003$

[a] $R_1 = \Sigma||F_o| - |F_c||/\Sigma|F_o|$, $wR_2 = [\Sigma w(F_o^2 - F_c^2)^2/\Sigma_w(F_o^2)^2]^{1/2}$

Table S14. Selected bond lengths (Å) and bond angles (°) for complexes **α-DyCl-UV and β-DyCl-UV**.

α-DyCl-UV			
Dy1-O1	2.306(4)	O4-Dy1-Cl3	93.60(10)
Dy1-O4	2.277(4)	O4-Dy1-O1	90.35(14)
Dy1-O7	2.290(3)	O4-Dy1-O7	176.28(12)
Dy1-Cl1	2.609(1)	O7-Dy1-Cl1	89.58(9)
Dy1-Cl2	2.628(1)	O7-Dy1-Cl2	94.57(9)
Dy1-Cl3	2.614(1)	O7-Dy1-Cl3	89.77(9)
O1-Dy1-Cl1	90.26(10)	O7-Dy1-O1	86.29(13)
O1-Dy1-Cl2	85.41(10)	Cl1-Dy1-Cl2	173.79(4)
O1-Dy1-Cl3	176.05(10)	Cl1-Dy1-Cl3	89.51(4)
O4-Dy1-Cl1	92.03(10)	Cl2-Dy1-Cl3	95.12(5)
O4-Dy1-Cl2	83.56(10)		
β-DyCl-UV			
Dy1-O1	2.293(6)	O4-Dy1-Cl3	88.45(16)
Dy1-O4	2.248(5)	O4-Dy1-O1	89.50(2)
Dy1-O7	2.252(6)	O7-Dy1-Cl1	89.73(17)
Dy1-Cl1	2.610(2)	O7-Dy1-Cl2	90.78(16)
Dy1-Cl2	2.642(2)	O7-Dy1-Cl3	93.59(16)
Dy1-Cl3	2.613(2)	O7-Dy1-O1	88.40(2)
O1-Dy1-Cl1	85.90(16)	O7-Dy1-O4	176.94(19)
O1-Dy1-Cl2	83.38(15)	Cl1-Dy1-Cl2	169.25(8)
O1-Dy1-Cl3	177.97(15)	Cl1-Dy1-Cl3	94.22(8)
O4-Dy1-Cl1	92.40(17)	Cl2-Dy1-Cl3	96.47(7)
O4-Dy1-Cl2	86.72(17)		

VII. References:

1 D.-K. Cao, Y.-W. Gu, J.-Q. Feng, Z.-S. Cai and M. D. Ward, *Dalton Trans.*, 2013, **42**, 11436–11444.

2 O. Kahn, Molecular Magnetism, Wiley-VCH: New York., 1993.

3 SAINT, Program for Data Extraction and Reduction, Siemens Analytical X-ray Instruments, Madison, WI, 1994–1996.

4 (a) O. V. Dolomanov, L. J. Bourhis, R. J. Gildea, J. A. K. Howard and H. Puschmann, *J. Appl. Cryst.*, 2009, **42**, 339–341; (b) L. Krause, R. Herbst-Irmer, G.M. Sheldrick and D. Stalke, *J. Appl. Cryst.*, 2015, **48**, 3–10.

5 I. F. Galván, M. Vacher, A. Alavi, C. Angeli, F. Aquilante, J. Autschbach, J. J. Bao, S. I. Bokarev, N. A. Bogdanov, R. K. Carlson, L. F. Chibotaru, J. Creutzberg, N. Dattani, M. G. Delcey, S. S. Dong, A. Dreuw, L.F reitag, L. M. Frutos, L. Gagliardi, F. Gendron, A. Giussani, L. González, G. Grell, M. Y. Guo, C. E. Hoyer, M. Johansson, S. Keller, S. Knecht, G. Kovacevic, E. Källman, G. L. Manni, M. Lundberg, Y. J. Ma, S. Mai, J. P. Malhado, P. Å. Malmqvist, P. Marquetand, S. A. Mewes, J. Norell, M. Olivucci, M. Oppel, Q. M. Phung, K. Pierloot, F. Plasser, M. Reiher, A. M. Sand, I. Schapiro, P. Sharma, C. J. Stein, L. K. Sørensen, D. G. Truhlar, M. Ugandi, L. Ungur, A. Valentini, S. Vancoillie, V. Veryazov, O. Weser, T. A. Wesołowski, P. Widmark, S. Wouters, A. Zech, J. P. Zobel and R. Lindh, *J. Chem. Theory Comput.*, 2019, **15**, 5925–5964.

6 L. F. Chibotaru, L. Ungur and A. Soncini, Angew. Chem. Int. Ed., 2008, **47**, 4126–4129.

7 L. Ungur, W. Heuvel and L. F. Chibotaru, *New J. Chem.*, 2009, **33**, 1224–1230.

8 L. F. Chibotaru, L. Ungur, C. Aronica, H. Elmoll, G. Pilet and D. Luneau, *J. Am. Chem. Soc.*, 2008, **130**, 12445–12455.

9 D. Aravena, *J. Phys. Chem. Lett.*, 2018, **9**, 5327–5333.

10 B. Yin and C.-C. Li, *Phys. Chem. Chem. Phys.*, 2020, **22**, 9923–9933.